Heliyon 8 (2022) e11999

Contents lists available at ScienceDirect

Heliyon

journal homepage: www.cell.com/heliyon

Research article

Crashworthiness analysis and design of a sandwich composite electric bus structure under full frontal impact

Pattaramon Jongpradist [a,b], Napassakorn Saingam [b], Ploypimol Tangthamsathit [b], Panittha Chanpaibool [b], Jariyavadee Sirichantra [c], Sontipee Aimmanee [d,*]

[a] Mobility and Vehicle Technology Research Center, King Mongkut's University of Technology Thonburi, 126 Pracha Uthit Rd., Bang Mod, Thung Khru, Bangkok, 10140, Thailand

[b] Department of Mechanical Engineering, Faculty of Engineering, King Mongkut's University of Technology Thonburi, 126 Pracha Uthit Rd., Bang Mod, Thung Khru, Bangkok, 10140, Thailand

[c] Department of Science Service, Ministry of Higher Education, Science, Research and Innovation, 75/7 Rama VI Road, Ratchathewi, Bangkok, 10400, Thailand

[d] Advanced Materials and Structures Laboratory (AMASS), Center for Lightweight Materials Design and Manufacturing, Department of Mechanical Engineering, Faculty of Engineering, King Mongkut's University of Technology Thonburi, 126 Pracha Uthit Rd., Thung Khru, Bangkok, 10140, Thailand

ARTICLE INFO

Keywords:
Crash analysis
Sandwich composite structure
Occupant injury
Crashworthiness
Finite element analysis

ABSTRACT

The transition toward sustainable transportation includes adopting ecofriendly electric vehicles in public transport, which reduces greenhouse gas emissions and increases energy efficiency. One of the critical features in fuel economy improvement of electric vehicles lies in lightweight structural design. Nevertheless, the crashworthiness of the structures of the vehicles and the safety of passengers must be guaranteed in the attempt of mass reduction because the crash of large vehicles such as buses usually costs many lives. This paper, therefore, aims to present an in-depth analysis of the impact behavior of a lightweight monocoque sandwich composite microbus body under full-frontal crash conditions. The bus structure, made of a high-density polyurethane foam core and woven glass fabric-epoxy face sheets, was modeled and simulated via LS-DYNA dynamic analysis using strength-based Chang-Chang criteria to characterize the failure mechanism of the structure and investigate intrusion into the passenger survival space. Under front collision, the front panel, A-pillars, and front sidewalls of the original bus were found to be extensively damaged in the compressive fiber mode. Based on the 50th percentile male dummy anthropometric parameters, injury indices of 0-5 intervals were proposed to evaluate occupant injury risks. The maximum front and side intrusion into the specified safety space under a maximum impact speed of 50 km/h is 208 mm at the front panel and 221 mm at the sidewall, indicating high injury indices of 3.59 and 4.81, respectively. The effects of stiffeners reinforced in the front panel and foam core thicknesses in the sidewalls, floor, and bottom parts on crashworthiness improvement were thoroughly discussed. The improved bus design can significantly enhance the safety of the occupants with a minimal increase in structural weight of merely 35.6 kg. An effective vehicle safety design under full frontal collision is presented.

1. Introduction

Battery electric vehicles are becoming widely used in public transport worldwide as an environmentally friendly alternative toward sustainable mobility, which benefits greenhouse gas emission reduction and energy efficiency. One of the critical features for increasing fuel economy improvement lies in lightweight structural design (Chu and Majumdar, 2012). A 10% reduction in vehicle weight can result in a 6% to 8% increase in energy consumption efficiency (Joost, 2012; Luk et al., 2017). Sandwich composite materials are perfectly eligible for this application due to their manufacturing tailorability, high strength-to-weight ratio, specific modulus, fatigue resistance, and energy absorption (Pavlović et al., 2020; Fantuzzi et al., 2021).

Several researchers have employed sandwich composite monocoque structures in the structural design of electric buses in recent years. Ning et al. (2007) designed a mass transit bus-body panel using a sandwich composite with E-glass fiber/polypropylene (glass/PP) face sheets and a PP honeycomb core in which 55% weight saving was achieved

* Corresponding author.
E-mail address: sontipee.aim@kmutt.ac.th (S. Aimmanee).

https://doi.org/10.1016/j.heliyon.2022.e11999
Received 17 July 2022; Received in revised form 10 September 2022; Accepted 23 November 2022

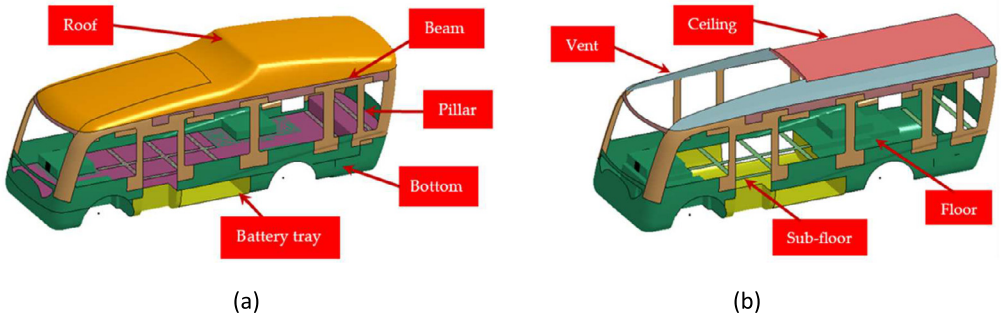

Fig. 1. Components of the microbus monocoque; (a) exterior components, (b) interior components.

compared to a conventional bus with metal frames. Testoni (2015) explored the feasibility of manufacturing and production costs of five different monocoque solutions made of carbon, glass, and natural fiber and their combinations. Kunakorn-ong et al. (2020) proposed a novel methodology to characterize the structural behavior of monocoque sandwich composite buses with varying core and face thicknesses based on bending- and torsion-stiffness requirements and rollover safety.

Aside from performance and efficiency, vehicle structural design must also be concerned with the protection and safety of the occupants in the case of crash accidents. According to figures reported by National Highway Traffic Safety Administration (2021), 63.9 percent of fatal collisions occurred during the frontal crash of a vehicle, and rollovers were more likely to happen to heavy vehicles than passenger cars. Design for bus crashworthiness from rollover accidents regarding United Nations Economic Commission of Europe (UNECE) Regulation No. 66 (2007) has gained much attention in recent years (Kwasniewski et al., 2009; Kongwat et al., 2020; Kunakorn-ong and Jongpradist, 2020; Seyedi et al., 2019). Regulations for occupant crash protection in heavy vehicle frontal collisions include pendulum impact tests based on UNECE Regulation No. 29 (2014) and front impact to rigid barrier according to Federal Motor Vehicle Safety Standard (FMVSS) no. 208 (National Highway Traffic Safety Administration, 2011). However, crashworthiness assessment of bus structures under frontal collision is scarce. In addition, vehicle passive safety analyses were primarily performed for metallic structures (e.g., Jongpradist et al., 2015; de Meira et al., 2016), but few have been conducted for sandwich composite bus structures due to their complex damage behaviors during a crash (Hartley, 2018). Thus, knowledge of the crash behavior of composite buses is very limited in the literature. Only studies on simple sandwich panels have been conducted by researchers. Experimental results indicated that sandwich panels made from glass fiber face sheets and polystyrene foam cores collapsed progressively, exhibiting high energy absorption capabilities (Tarlochan et al., 2012). Wang et al. (2018) compared the effects of failure criteria on the numerical responses of composite laminates subject to low-velocity impact. The expressions of the Chang-Chang and Hashin criteria show acceptable agreement with the experimental data with reasonable computational cost.

To fill the gap in the research body, the present study investigates monocoque sandwich composite microbus behavior under full-frontal crashes using finite element simulation via LS-DYNA software. Two injury indices defined from the level of intrusion in the residual space are proposed to gauge the collision severity to a male driver dummy. Four kinds of crashworthiness improvement were thoroughly analyzed to assess the effectiveness of each strategy. Additionally, presented in the Appendix, the material model and damage behavior of composite laminates were validated through impact drop tests with comparable specific impact energy to the frontal bus collision. The damage mechanism of the whole bus structure and the possibility of occupant injury were evaluated. Finally, design guidelines are proposed to enhance the crashworthiness performance of the vehicle structure.

Table 1. Material properties of composite materials.

Properties	G400	G600	C200
Longitudinal modulus (GPa)	18.0	16.3	78.5
Transverse modulus (GPa)	18.0	16.3	78.5
In-plane shear modulus (GPa)	2.22	2.94	2.12
Poisson's ratio	0.1	0.04	0.052
Longitudinal tensile strength (MPa)	415	502	411
Longitudinal compressive strength (MPa)	200	203	371
Transverse tensile strength (MPa)	415	502	411
Transverse compressive strength (MPa)	200	203	371
In-plane shear strength (MPa)	75	105	105
Density (kg/m^3)	1,588	1,717	1,336

2. Frontal crash analysis of the composite microbus

2.1. Original microbus design

The original microbus design is based on the electric monocoque sandwich-structured microbus from Kunakorn-ong et al. (2020). The bus structure was designed and optimized according to bending stiffness, torsional stiffness, natural frequency requirements, and the UNECE R66 rollover standard. The 24-seat microbus is 2.4 meters wide, 3.2 meters high, and 7.8 meters long. The microbus was divided into nine components: roof, vent, ceiling, pillar, beam, floor, subfloor, battery tray, and bottom, as shown in Fig. 1. All parts except for the roof are sandwich panels consisting of H100 foam cores with different thicknesses and composite E-glass fiber/epoxy face sheets with different ply orientations and stacking sequences. The lay-up configuration in each component is displayed in Fig. 2. In the original design, E-glass fiber fabrics with densities of 400 g/m^2 and 600 g/m^2, so-called G400 and G600, respectively, were primarily designated in the main components. The plain-weave carbon fiber with a surface density of 200 g/m^2 (C200) was used to reinforce the battery tray and subfloor parts in which higher bending stiffness is particularly needed.

2.2. Modeling of front crash simulation

Full-frontal crash simulation of the microbus was performed by nonlinear explicit finite element analysis using LS-DYNA software. The simulation was set up based on the standard of the vehicle impact testing FMVSS 208 as displayed in Fig. 3. The electric microbus structural model is meshed using a Belytschko-Tsay shell element with an element size of 30 mm, comprising 101,850 nodes and 104,815 elements. Based on the Reissner-Mindlin kinematic assumption, the element formulation ELFORM was set to 2 with one-point and bilinear nodal integration. This type of element was chosen because it is economical and robust for impact analysis (LS-DYNA, 2020). The mechanical properties of the composite materials in Table 1 were defined as MAT054 with enhanced composite damage. The 2-way fiber option was specified to represent the behavior of woven fabric. The material model for the H100 foam core was assigned as MAT063 crushable foam. By default, LS-DYNA shells imply uniform transverse shear strain, which

Vent	Battery tray	Ceiling	Bottom	Pillar	Floor	Beam	Subfloor	Roof
G600[0/90]$_7$	C200[0/90]$_3$	G600[0/90]$_7$						
	C200[45/-45]$_4$	G600[45/-45]$_7$						
G600[45/-45]$_4$	G600[0/90]$_9$	G400[0/90]$_6$	G400[0/90]$_6$	G400[0/90]$_9$	G400[0/90]$_4$	G400[0/90]$_8$		
	G600[45/-45]$_8$	G400[45/-45]$_5$	G400[45/-45]$_8$	G600[0/90]$_{10}$	G400[45/-45]$_5$	G400[45/-45]$_6$		
H100 t = 30 mm	H100 t = 50 mm	H100 t = 50 mm	H100 t = 50 mm	H100 t = 40 mm	H100 t = 40 mm	H100 t = 40 mm	H100 t = 5 mm	G400[0/90]$_{10}$
G600[45/-45]$_4$	G600[45/-45]$_8$	G400[45/-45]$_5$	G400[45/-45]$_8$	G600[0/90]$_{10}$	G400[45/-45]$_5$	G400[45/-45]$_6$	C200[0/90]$_4$	
	G600[0/90]$_9$	G400[0/90]$_6$	G400[0/90]$_6$	G400[0/90]$_9$	G400[0/90]$_4$	G400[0/90]$_8$		
G600[0/90]$_7$	C200[45/-45]$_4$	G600[45/-45]$_7$						
	C200[0/90]$_3$	G600[0/90]$_7$						

Fig. 2. Layup configuration for each component of the microbus.

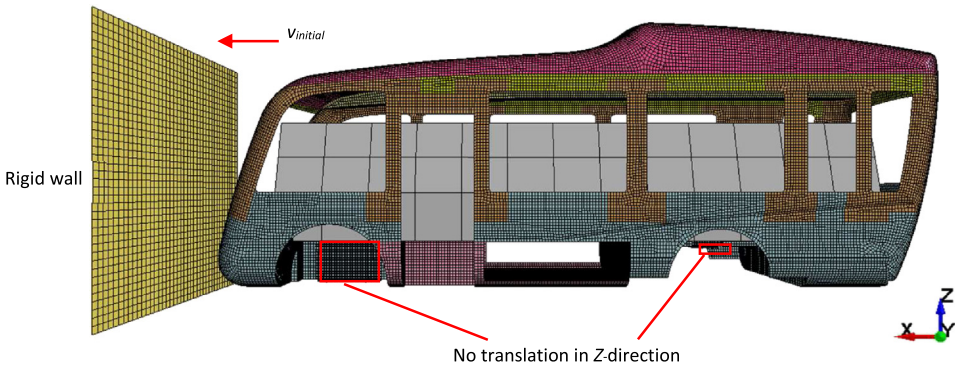

Fig. 3. Finite element model of a microbus under full-front crash into a rigid wall barrier.

is not valid for relatively thick foam core composites or stack-up laminates with diverse materials and stiffness varying through the thickness. Therefore, *PART_COMPOSITE was used to define the shell integration points through the thickness of the composite sandwich structure. The BETA angles were also employed to identify the initial orientation of the material coordinate system. Using one integration point through thickness for each fiber orientation in the composite face and one point through the foam core thickness was proven cost-effective and provides accurate results (Jongpradist et al., 2021). In addition, laminated shell theory was activated for sandwich composites with soft cores by using LAMSHT = 1 in *CONTROL_SHELL to remove the assumption of uniform shear strain through the shell thickness.

The weights of nonstructural components, i.e., axle systems, seating, passengers, air conditioning systems, batteries, doors, and windows, were allocated to the finite element model as uniformly distributed mass elements at the parts listed in Table 2. The microbus was constrained against translation in the Z-direction at the positions of the wheel axles. The automatic surface-to-surface contact interaction was assigned between the microbus frontal parts and the rigid wall barrier, whereas self-contact interaction was also specified for all bus parts. To simulate the vehicle crash into the rigid wall, the initial velocity of 50 kilometers per hour in the +X-direction was applied to the entire microbus model. The crash analysis was terminated after the collision ended at 170 ms, when the entire initial kinetic energy transformed into the internal strain energy of the bus. To assess the failure mode of the composite structure, history variables defining fiber and matrix damage conditions must be collected via *DATABASE EXTENT BINARY. The stress-based Chang-Chang criterion (LS-DYNA, 2020) was applied to predict the failure mode of the laminate. The failure conditions in

Table 2. Additional mass allocated to the finite element model.

Items	Location	Weight (kg)
Rear axle system	Bottom	950
Front axle system	Bottom	482
12 Double seats and driver seat	Floor	407
Driver and 24 Passengers	Floor	1,875
Air conditioning system	Ceiling	180
Battery	Battery tray	1,536
Passenger doors and windows	Bottom	460
Total		5890

the a- and b-directions corresponding to the warp and weft directions, respectively, can be expressed in Equations (1) to (5).

For the tensile fiber mode:

when

$$\sigma_{aa} > 0, \quad e_{fa}^2 = \left(\frac{\sigma_{aa}}{X_t}\right)^2 + 0.5\left(\frac{\sigma_{ab}}{S_c}\right)^2 - 1 \begin{cases} e_{fa}^2 < 0 : \text{elastic} \\ e_{fa}^2 \geq 0 : \text{failed} \end{cases} \tag{1}$$

and when

$$\sigma_{bb} > 0, \quad e_{fb}^2 = \left(\frac{\sigma_{bb}}{X_t}\right)^2 + 0.5\left(\frac{\sigma_{ab}}{S_c}\right)^2 - 1 \begin{cases} e_{fb}^2 < 0 : \text{elastic} \\ e_{fb}^2 \geq 0 : \text{failed} \end{cases} \tag{2}$$

For the compressive fiber mode:

when

$$\sigma_{aa} < 0, \quad e_{ca}^2 = \left(\frac{\sigma_{aa}}{X_c}\right)^2 - 1 \begin{cases} e_{ca}^2 < 0 : \text{elastic} \\ e_{ca}^2 \geq 0 : \text{failed} \end{cases} \tag{3}$$

and when

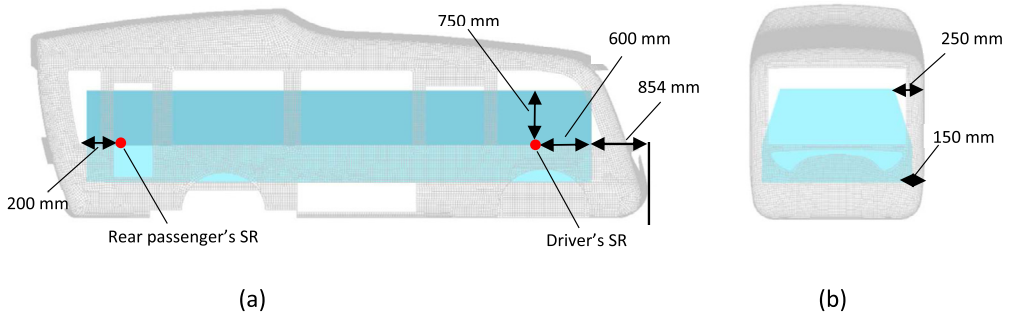

Fig. 4. Residual space of the microbus; (a) side view, (b) front view (SR stands for seat reference).

$$\sigma_{bb} < 0, \quad e_{cb}^2 = \left(\frac{\sigma_{bb}}{X_c}\right)^2 - 1 \quad \begin{cases} e_{cb}^2 < 0 : \text{elastic} \\ e_{cb}^2 \geq 0 : \text{failed} \end{cases} \tag{4}$$

For the shear matrix mode:

$$e_m^2 = \left(\frac{\sigma_{ab}}{S_c}\right)^2 - 1 \qquad \begin{cases} e_m^2 < 0 : \text{elastic} \\ e_m^2 \geq 0 : \text{failed} \end{cases} \tag{5}$$

where σ_{ij} are the stress components and e_f, e_c, and e_m represent the failure conditions in fiber tension, fiber compression, and matrix shearing, respectively. X_T is the tensile strength in both directions. S_c is the in-plane shear strength, and X_c is the compressive strength.

2.3. Residual space and injury index definitions

For safety analysis of the bus structure under frontal collision, a passenger survival space above the floor, the so-called residual space, was created in the finite-element simulation according to the UN-ECE R66 regulation for bus crashworthiness under rollover accidents (UNECE, 2007). The safety of the occupants is protected when no intrusion or penetration of structural parts occurs to the residual space during or after the collision. The residual space is defined as two-dimensional rigid blue surfaces assembled into the shape of a trapezoidal prism on the top of a rectangular box, whose reference dimensions are given in Figs. 4(a) and 4(b).

To further evaluate the accident severity representing the threat to the occupants' lives, two injury indices were established based on the maximum intrusion of the structural parts to the dimensions of the 50th percentile male occupant dummy. They were classified on a scale of 0 to 5, where 0 indicates no occupant injury and 5 designates critical to fatal injury. The first injury index I_f is adopted to measure the injury severity from frontal intrusion. The maximum intrusion of the front structure into the residual space in the X-direction is denoted by x_{int}, which is depicted in Fig. 5(a). The positive value of x_{int} specifies intrusion into the residual space. In contrast, the negative sign of x_{int} means that the deformation profile of the front structure moves away from the safety area. The value I_f was calculated according to Equation (6), where A_f is the longitudinal distance between the residual space boundary and the dummy's toe, whereas B_f denotes the longitudinal distance between the residual space boundary and the dummy's chest.

$$I_f = \begin{cases} 0, & \text{for } x_{int} \leq -A_f \\ \frac{x_{int}}{A_f} + 1, & \text{for } -A_f < x_{int} \leq 0 \\ \frac{4x_{int}}{B_f} + 1, & \text{for } 0 < x_{int} \leq B_f \\ 5, & \text{for } x_{int} > B_f \end{cases} \tag{6}$$

As seen in Equation (6), the injury index I_f is equal to 0 when none of the deformed front structure touches any parts of the driver dummy. If the maximum deformation of the front structure is more than $-A_f$ until the rim of the residual space area, I_f is equal to one, and minor injuries are expected. However, critical injuries occur when the deformed structure reaches the position of the chest of the driver so that I_f reaches the maximum value of five. Note that piecewise linear scales are applied in the equation when the intrusion x_{int} is in the 0-5 interval.

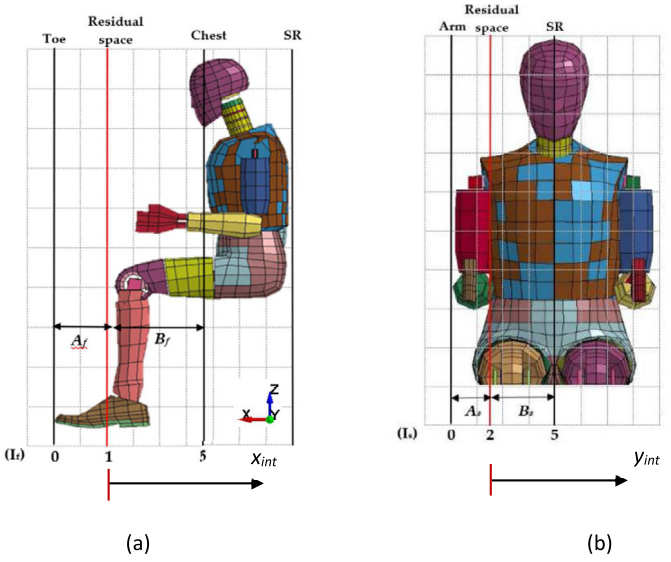

Fig. 5. Definition of Injury Indices to the dimensions of the 50th percentile male dummy; (a) frontal injury index, I_f, (b) side injury index, I_s, (SR stands for seat reference).

Similarly, the second injury index for side intrusion I_s can be assessed by the maximum intrusion of the side structure into the survival space in the Y-direction during the crash, y_{int} shown in Fig. 5(b). The index I_s was evaluated according to Equation (7).

$$I_s = \begin{cases} 0, & \text{for } y_{int} \leq -A_s \\ -\frac{2y_{int}}{A_s}, & \text{for } -A_s < y_{int} \leq 0 \\ \frac{3y_{int}}{B_s} + 2, & \text{for } 0 < y_{int} \leq B_s \\ 5, & \text{for } y_{int} > B_s \end{cases} \tag{7}$$

In the above equation, A_s is the transverse distance between the residual space boundary and the outermost part of the dummy's side. B_s is the transverse distance from the residual space boundary to the driver's midbody. For this index, moderate injuries with I_s of 2 are expected when the side structure intrudes into the residual space, whereas fatal injuries occur when I_s is equal to 5, at which the intrusion reaches the midbody of the dummy. Again, piecewise linear interpolations are also applied for calculating in-between intrusion values. Note that other crash influences on passenger injury, such as the Head and Neck Injury Criteria, are not considered in this paper.

3. Results of the original model

Microbus frontal crashes were analyzed under an initial velocity of 50 km/h. In this work, the quantities A_f, B_f, A_s, and B_s are 205,

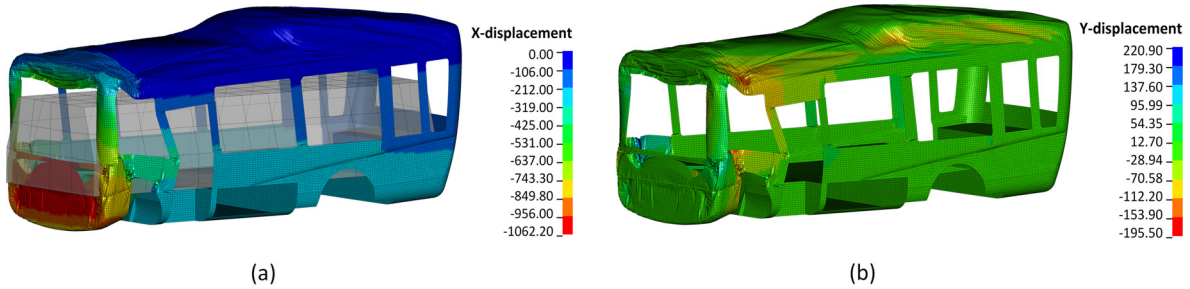

Fig. 6. Deformation of the microbus under a 50 km/h full-front crash; (a) X-displacement (b) Y-displacement.

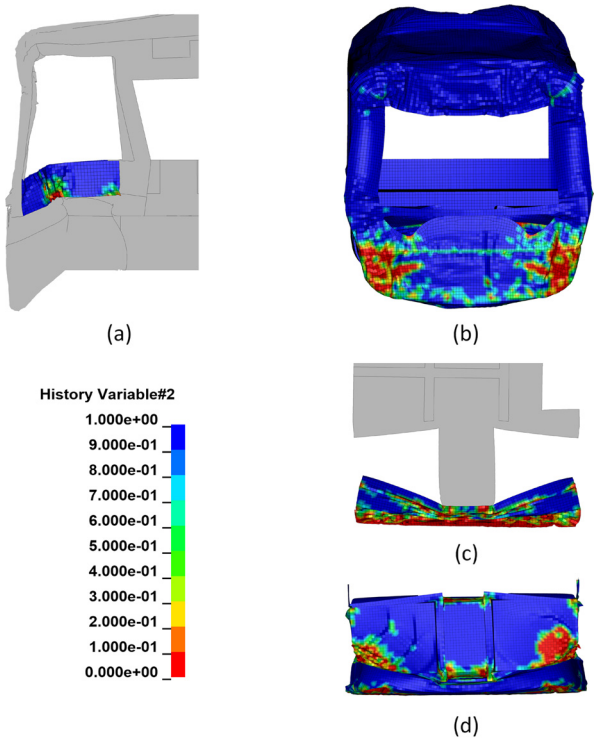

Fig. 7. Compressive fiber damage in different parts of the original model; (a) side view of the sidewall, (b) front view of the front bottom, (c) top view of the front floor, (d) top view of the front bottom.

320, 162, and 63 mm, respectively. Figs. 6(a) and 6(b) display the X- and Y-displacements of the deformed bus structure relative to the rearmost component after frontal impact, such that the net value of permanent deformations can readily be seen and interpreted. The figure also includes the residual space to conveniently gauge the level of crashworthiness. The maximum intrusion in the residual space in the X-direction is 208 millimeters on the front panel. This deformation corresponding to the injury index I_f of 3.59 indicates that the front panel is collapsed into the driver at the position of the driver's inner thigh and conceivably causes a serious injury to the driver. The maximum Y-deformation occurs on the sidewall between the A-pillar and B-pillar with a maximum intrusion of 221 millimeters. In this transverse direction, the injury index is 4.81, representing sidewall penetration into the residual space to the middle of the occupant's chest. Thus, the original model of the microbus is considered highly unsafe for the driver in the event of a full-frontal collision at a speed of 50 km/h.

Failure of the bus structure is observed mainly at the frontal and sidewall structures in a compressive fiber mode. Fig. 7 shows the contour of the damage parameter of the compressive fiber mode (History variable #2) at the sidewall (Fig. 7(a)), the frontal part of the bottom component dubbed the front bottom (Fig. 7(b) and 7(d)), and the frontal part of the floor component dubbed the front floor (Fig. 7(c)). The damage parameter of unity (shown in blue in the scale bar) represents the intact parts in which the stresses are in the elastic range, so no failure occurs. The parameter is equal to zero (shown in red) when the material fails completely due to excessive compressive stress in fibers according to the Chang-Chang criteria stated in Equations (3) and (4). These fully impaired parts cannot withstand any additional load or absorb more impact energy from the crash. Crash energy absorption by each component of the microbus was also analyzed, showing consistent results with the damage behavior discussed earlier.

At slower initial crash velocities of 20 to 40 km/h, deformations of the front panel and A-pillar are marginal, with no intrusion of any bus parts into the residual space. However, the front panel has been damaged in all failure modes at the initial bus speed of 40 km/h, with the initiation of damage detected at the outer ply of the sandwich face of the front panel. The most extensive damage is again in the compressive fiber mode. The main components in crash energy absorption are the front bottom and front floor, where almost 80% of 218 kJ crash energy is absorbed at 40 km/h. For the initial crash speed of 50 km/h, the front-bottom component absorbs most of the collision energy of 340 kJ, which is 47.3% of the total kinetic energy, while the front floor component absorbs approximately 184 kJ or 25.6%. The analysis results show that energy from the frontal crash can hardly dissipate to the remaining elements of the structure. To enhance the crashworthiness of the microbus for passenger safety, the structural stiffness of the frontal parts should be adjusted, and additional energy-dissipating components should be incorporated.

4. Study on crashworthiness improvement

4.1. Modified microbus design

According to the full-frontal crash analysis of the original design, severe damages are observed at the front panel of the bottom, the front floor component of the driver's compartment, and the sidewall. To improve the crashworthiness of the bus structure, the effects of adjusting the foam core thicknesses of the sandwich composites of these parts and adding stiffeners of different thicknesses to the front panel were studied, along with the weight efficiency. The stiffener and the foam-core thicknesses were increased until intrusion to the residual space approached zero or the effects of changing the parameters were not weight-efficient because the insignificant change in intrusion is achieved. Fig. 8(a) shows the design of four G600-glass-fiber/epoxy stiffeners placed under the floor at the front panel and parallel to the bus length. The G600 glass fiber composite is used for this component due to its superior strength in compressive mode. Figs. 8(b), 8(c), and 8(d) illustrate the altered components of the front bottom, front floor, and sidewall in which the foam core thicknesses were increased to improve the bending stiffness of the parts. Apart from the modification in Fig. 8, the remaining lay-up configurations were kept the same as the original design. The effects of crashworthiness improvement of the structure are then evaluated based on the intrusion distance, the absorbed impact energy, and the weight difference.

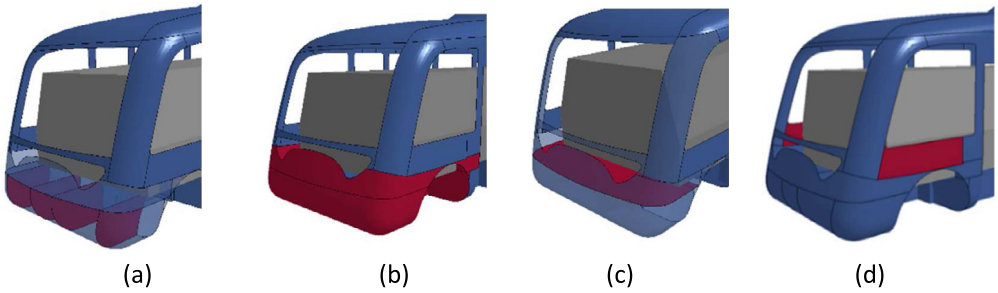

Fig. 8. Change in components to improve crashworthiness under frontal crash: (a) adding stiffeners, (b) increasing foam core thickness in front bottom (c) increasing foam core thickness in front floor (d) increasing foam core thickness in sidewall.

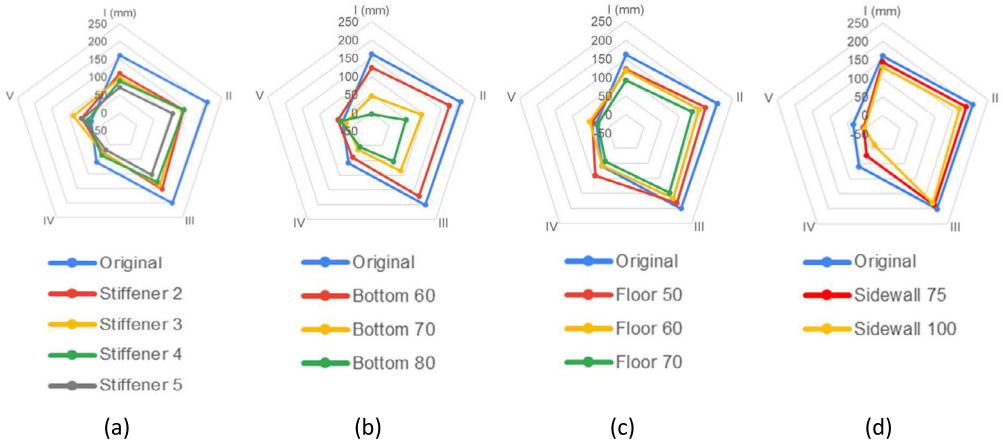

Fig. 9. Intrusion to residual space for five locations with varying thicknesses of (a) stiffeners, (b) front panel, (c) front floor, (d) sidewall. Case I in the radar chart is for X-intrusion at the front panel, case II for X-intrusion at the A-pillar on the driver's side, case III for X-intrusion at the A-pillar on the door's side, case IV for Y-intrusion at the driver sidewall, case V for Y-intrusion at the door sidewall.

Fig. 9 illustrates the maximum intrusion to the residual space in the X- and Y-directions for five cases. Fig. 9(a) shows that adding the stiffeners can efficiently decrease the maximum intrusion in the X-axis, which occurs at the frontal parts (case I), and at the A-pillars on the driver's side and door's side (cases II and III, respectively). In addition, the intrusions are lessened with the thickness increment but not as significant as those resulting from the 2-mm stiffeners. Nevertheless, adding stiffeners does not benefit a substantial reduction in Y-axis intrusion at the driver sidewall (case IV). This addition of stiffeners even causes larger Y-intrusion displacements at the door sidewall (case V).

The effects of varying the foam core thicknesses for different components, i.e., the front bottom, front floor, and sidewall, on residual space intrusion are illustrated in Figs. 9(b), 9(c), and 9(d), respectively. Unlike adding stiffeners to the front panel, increasing the foam core thicknesses can reduce the intrusion in both the X- and Y-directions. Fig. 9(b) shows that increasing the foam core thickness of the front bottom by 30 mm from the original design (totally equal to 80 mm) can significantly reduce the intrusions of the front panels and the A-pillars up to 55%. The Y-intrusion of the driver sidewall can also be slightly diminished, while no influence is noticed on the door side. Fig. 9(c) shows results similar to Fig. 9(b), but the improvement in Fig. 9(c) is nonetheless noticeably lower. Finally, increasing the core thickness of the sidewall in Fig. 9(d) prominently reduces the intrusions in the Y-axis of both the driver and door sidewalls. However, it has a negligible effect on the deformation in the longitudinal direction of the front panel and A-pillars.

Next, the distributions of energy absorption in the affected components of the original and the improved bus models under frontal crashes are illustrated in Fig. 10. As previously seen, the frontal regions of the original bus model, which are directly in contact with the rigid wall, e.g., the front bottom, the front floor, and A-pillars, are damaged. According to Fig. 10(a), when the stiffeners are added to the structure, the absorbed energy of these parts evidently drops compared to the original model. The crash energy is transferred to the stiffeners as well as other components, such as the middle parts of the bottom and floor, resulting in minor deformations of the front structure. Moreover, Fig. 10(a) shows that the increased foam core thickness of the front bottom elevates the portion of the energy absorption in the front bottom and reduces the energy in the front floor. At the same time, the crash energy is slightly dissipated to the other structural components. Comparatively, Fig. 10(b) shows the results of increasing foam core thickness of the front floor and sidewall. In this case, the energy absorption of the front bottom is reduced, but the energy absorption of the front floor, the sidewalls, and the other noncontact parts is increased. Similarly, adding the foam core thickness of sidewalls offers higher energy absorption of the added part and the A-pillars. However, the front bottom and the front floor parts absorb less collision energy. Among the several improved designs, implementing stiffeners to the frontal part of the bus is the most efficient method to dissipate the crash energy from the front structure of the bus to the other structural components. Note that the energy dissipation in each component in the back parts, such as the ceiling, bottom back, floor back, and rear pillars, is less than 3% of the total impact energy.

Each of the structural alterations addressed above improves the crashworthiness of the microbus to a certain extent. However, the structural alterations cannot effectively reduce the intrusions to achieve sufficient safety at the five locations simultaneously. Consequently, a modified model was proposed by incorporating all four approaches. In the modified model, four 5-mm thick stiffeners were chosen. The foam core thicknesses of the front bottom, front floor, and sidewalls were increased to 70 mm, 50 mm, and 75 mm, respectively. The lay-up configurations of the modified model compared to the original design are

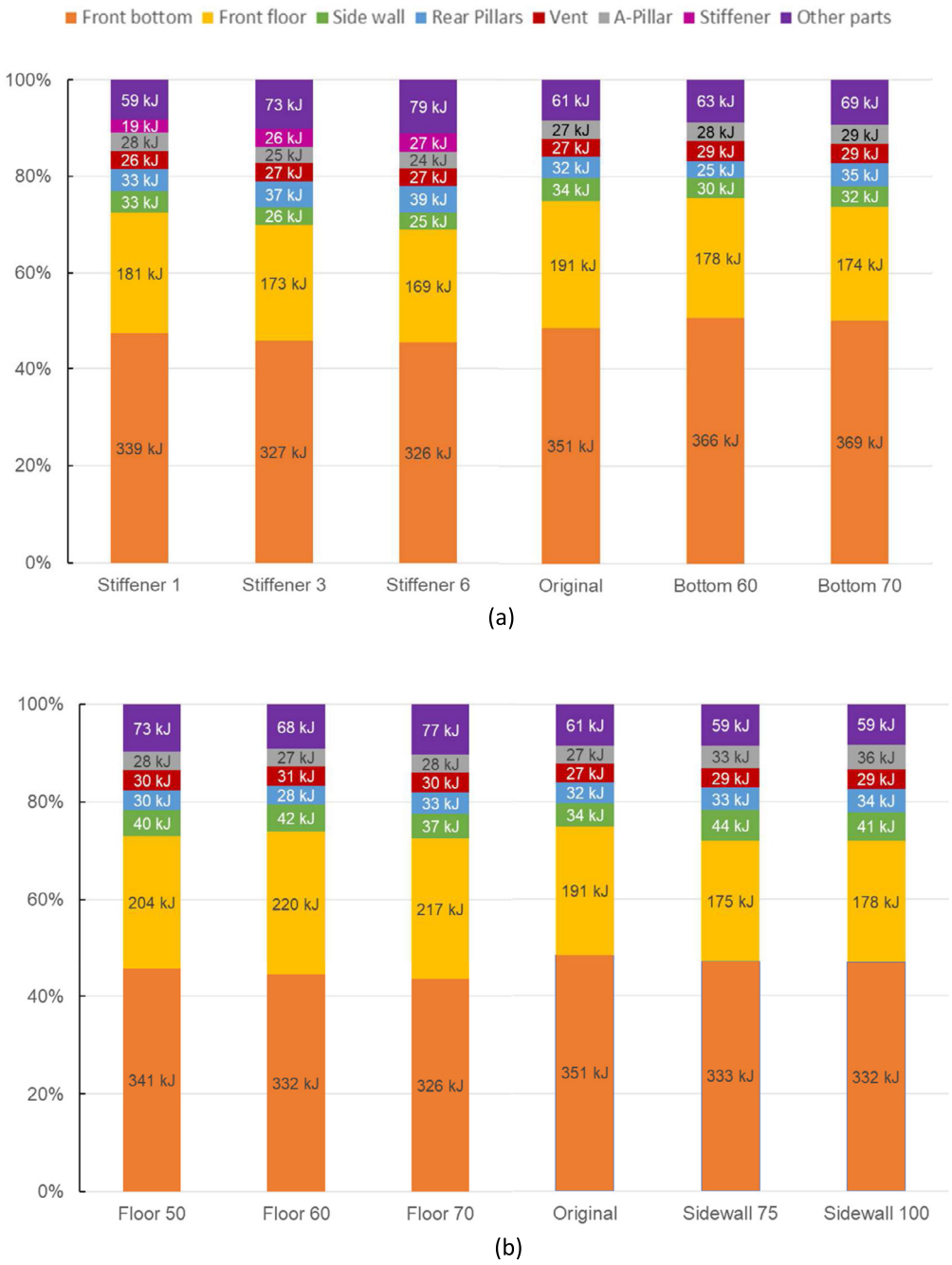

Fig. 10. Energy distribution in each component of the microbus; (a) stiffeners and Front bottom; (b) front floor and sidewall.

shown in Fig. 11. According to the figure, the overall structural weight of the modified microbus model is increased by 35.6 kg.

The intrusions obtained from the modified microbus with a velocity of 50 km/h and the corresponding injury indices are shown in Figs. 12(a) and 12(b), respectively. The modified model can prominently reduce the deformations of the microbus structure under frontal crashes, resulting in no maximum intrusions in either the X- or Y-axes beyond the residual space boundary. The injury indices from front intrusion I_f's are all less than 1.0, and the injury indices from side intrusion I_s's are all less than 2.0, indicating that no severe intrusion to the residual space occurs, and the modified microbus model significantly subsides with injury risks caused by frontal collision.

Further analyses were conducted on the dynamic responses and structural characteristics of the original and modified bus models under frontal crashes into a rigid wall at 50 km/h. The velocity-time histories at the CG of the bus in Fig. 13(a) demonstrate that the modified model can impede the crash velocity with a higher deceleration after the start of the crash incident at 48 ms, where the complete crash occurs at 144 ms compared to 175 ms for the original model. Then, the bus reflects from the wall with negative X-velocity due to the impact force. Although the average velocity of the floor front and the CG are marginally different, they exhibit the same trend for both models. The average decelerations of the original and modified microbus are 11.2 g and 14.8 g, respectively. Fig. 13(b) compares the impact force-frontal displacement curves for the two models. Strengthening the frontal structure creates a higher impact force at the earlier stage of the crash incident, while the average forces are quite similar afterward. The maximum deformation of the frontal structure can be significantly decreased by 195 mm. According to the energy consideration, the bus decelerations and external work induced from the area under the force-displacement curves

part	The original model				The modified model			
	Stiffeners	Front bottom	Front floor	Sidewalls	Stiffeners (4 pieces)	Front bottom	Front floor	Sidewalls
Lay-up configuration	no stiffener	G400 $[0/90]_6$		G400 $[0/90]_6$	G600 $[0/90]_8$ 5mm	G400 $[0/90]_6$		G400 $[0/90]_6$
		G400 $[\pm45]_8$	G400 $[0/90]_4$	G400 $[\pm45]_8$		G400 $[\pm45]_8$	G400 $[0/90]_4$	G400 $[\pm45]_8$
			G400 $[\pm45]_5$				G400 $[\pm45]_5$	
		H100 50mm	H100 40mm	H100 50mm		H100 70mm	H100 50mm	H100 75mm
		G400 $[\pm45]_8$	G400 $[\pm45]_5$	G400 $[\pm45]_8$		G400 $[\pm45]_8$	G400 $[\pm45]_5$	G400 $[\pm45]_8$
			G400 $[0/90]_4$				G400 $[0/90]_4$	
		G400 $[0/90]_6$		G400 $[0/90]_6$		G400 $[0/90]_6$		G400 $[0/90]_6$
Weight (kg)	-	1179.3	1170.5	17.2	11.4	1199.7 (+20.4kg)*	1172.4 (+1.9kg)*	19.1 (+1.9kg)*

Fig. 11. Comparison of the lay-up configuration and structural weight between the original and the modified design.

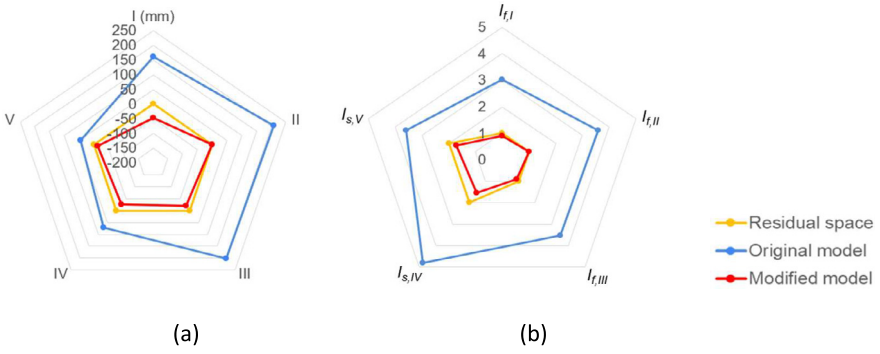

Fig. 12. Comparison of (a) intrusion to the residual space, and (b) the injury indices between the original and the modified design. Case I in the radar chart is for X-intrusion at the front panel, case II for X-intrusion at the A-pillar on the driver's side, case III for X-intrusion at the A-pillar on the door's side, case IV for Y-intrusion at the driver sidewall, case V for Y-intrusion at the door sidewall.

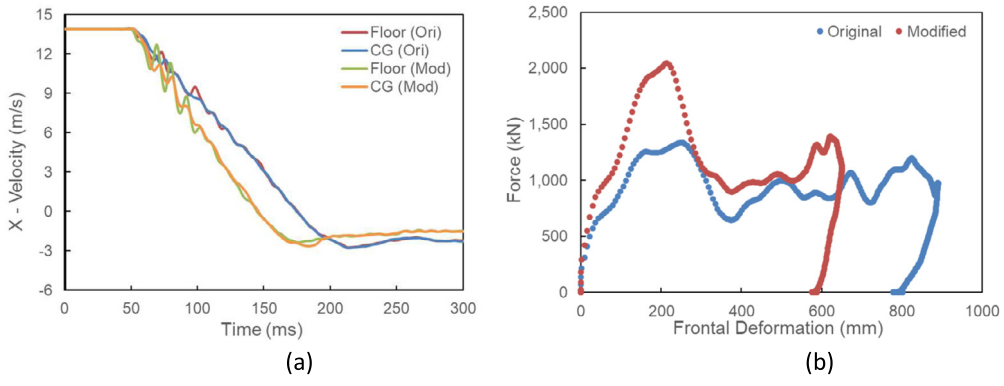

Fig. 13. Dynamic responses during frontal collision; (a) velocity-time histories, and (b) impact force-frontal displacement of the original and modified models.

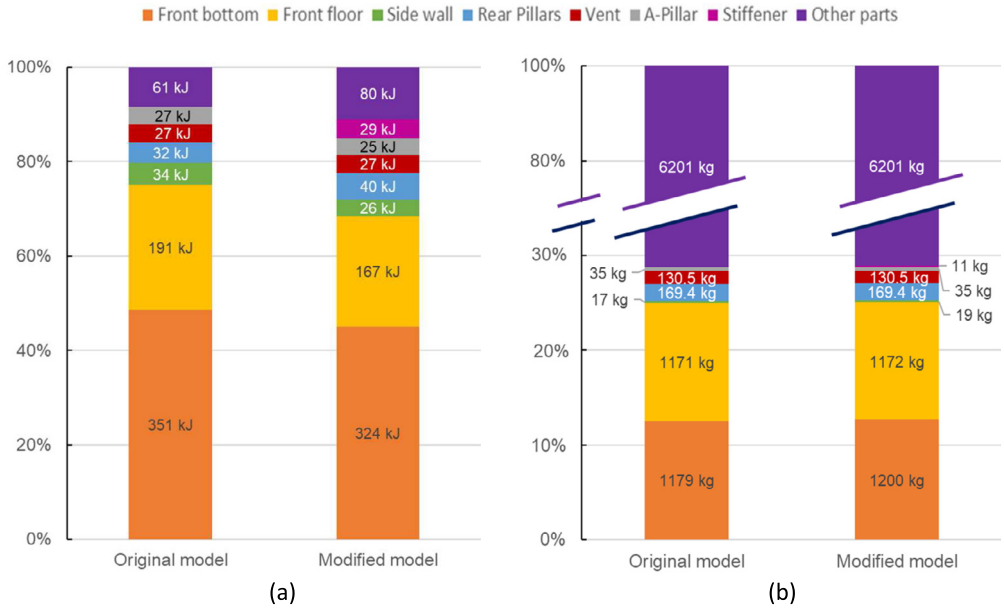

Fig. 14. Comparison between the original and modified designs: (a) energy absorption distribution, and (b) weight of each component.

can also imply the higher energy absorption in the modified microbus due to the presenting lower kinetic energy and higher work done of the modified model during the crash.

Fig. 14(a) directly compares the energy dissipation between the original and the modified model. In the modified model, the front components directly impact the rigid wall (i.e., the front bottom, front floor, A-pillars, and sidewalls) evidently absorb less impact energy during a crash. This behavior results from almost 10 percent of the total impact energy being successfully transferred to the other components, including the ceiling, bottom back, floor back, and other rear pillars. Therefore, damages in the front parts can be notably mitigated. Fig. 14(b) compares the component weight for the two models. The improved design of the parts with thicker foam cores has a minor increment of structural weight (1 percent increment) but can offer a substantial enhancement in the crashworthiness of the microbus structure.

Possible damages in the frontal parts of the modified bus are investigated in tensile fiber mode (History variable #1), compressive fiber mode (History variable #2), and shear matrix damage mode (History variable #3). Damages in all modes are observed to be more severe than the results of the original model, especially the compressive fiber damage. Fig. 15 shows that the damaged area in the compressive fiber mode is extensively expanded from the damaged area of the original model (Fig. 7), especially in the front bottom component (Figs. 15(b) and 15(d)). However, the areas of critical damage (History variable #2 = 0) in the front floor (Fig. 15(c)) and sidewalls (Fig. 15(a)) are slightly smaller. When the stiffness of the frontal sandwich structure is increased, the parts can withstand a crash incident more effectively, resulting in a larger damage area and less deformation.

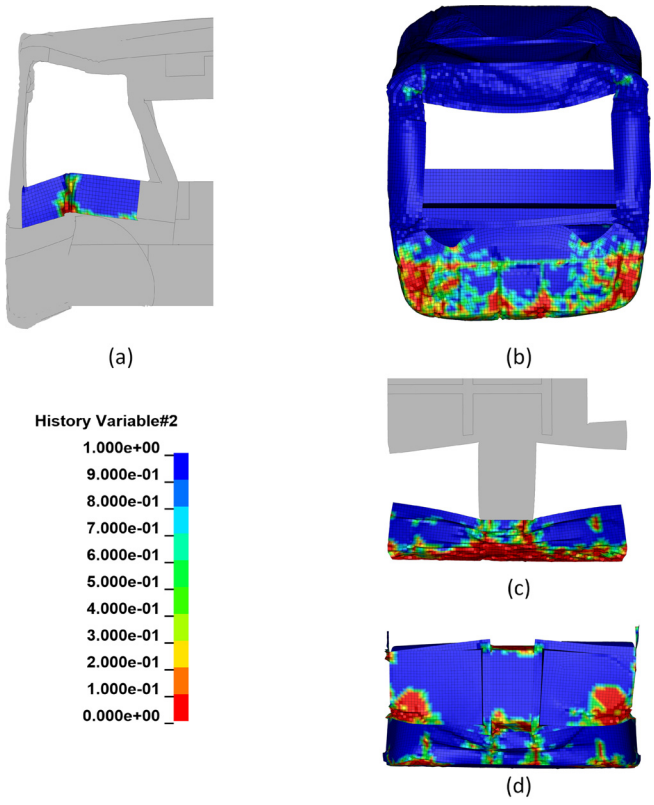

Fig. 15. The compressive fiber damage mode in the different parts; (a) side view of the sidewall, (b) front view of the front bottom, (c) top view of the front floor, (d) top view of the front bottom.

4.2. Lightweight design for passenger safety

The influences of varying the thickness of the stiffeners and thicknesses of the foam core in the front bottom and front floor components were further investigated to search for a wider crashworthiness design space. In this section, the closest clearance between the front panel and the specified residual space is used to indicate the level of passenger safety. For the cases considered, the higher the positive clearance is, the safer the passenger. Fig. 16 shows the relationship of the closest clearance versus the structural weight change resulting from the structural alterations. The baseline value, which represents zero frontal clearance (shown as the red triangle symbol in the figure), is obtained from the modified model. The baseline thicknesses of the corresponding components in the modified microbus are also displayed as the red numbers in the sequences of the varied thicknesses. Linear trendlines passing through the origin for each varied parameter can be fitted with a high correlation coefficient, showing its simplicity and sufficient accuracy. The least steep graph (yellow line) is detected by changing the foam-core thickness of the front bottom component, implying that when the safety space is already guaranteed, decreasing the front-bottom core

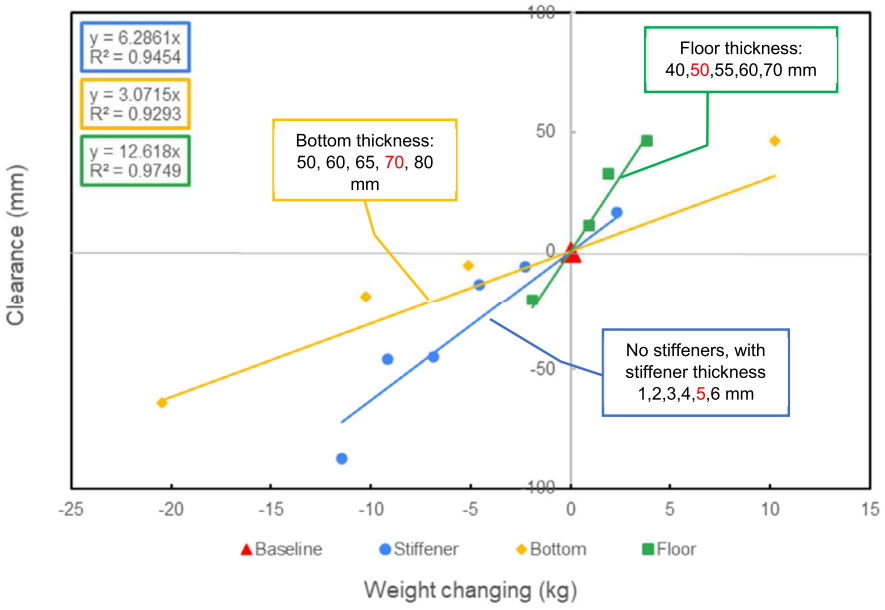

Fig. 16. The characteristics of adjusting the thicknesses of the foam core in four components.

thickness is suitable to gain the highest weight reduction with a small increment in frontal deformation. In contrast, the trendline attained by changing the core thickness of the front floor possesses the steepest slope, making it the most suitable variable for decreasing the front intrusion with a minimal increase in structural weight. Therefore, to increase safety factors and alleviate injury of the driver and passengers, adjusting the foam-core thickness of the front floor is the most effective way when weight saving is the crucial aspect in design improvement. Since the trend lines have a linear relationship, the clearance with multiple changes of the design parameters can be estimated by the linear combination of the provided trend lines in Fig. 16. In addition, because the current study was conducted in multiple simulation cases to cover the wide spectrum of design parameters, further investigation could use machine learning based on the available data to minimize the weight and cost of the electric composite bus.

5. Conclusions

This study involves crashworthiness analysis and design of a sandwich composite electric microbus. The damage parameters of the composite materials have been validated with the test specimens subjected to drop-weight impact, resulting in excellent agreement in the force-displacement relationship, hysteresis and damage behaviors between finite element simulation and experiments. The damage behavior of the bus under full-frontal crash simulation using LS-DYNA was thoroughly investigated. After the crash, the composite panels at the locations of direct impact to the rigid wall were significantly damaged in fiber compression. The frontal parts of the original structure were seriously deformed, resulting in intrusion into the survival space of the passenger and high injury risk to the occupants. Injury indices based on the intrusion distance on the front and the sides of the bus structure were defined to provide the indicators of injury risks under collision. Two main approaches were methodologically proposed to improve the crashworthiness of the microbus structure: first, adding stiffeners under the floor between the front panel and the front wheel, and second, increasing the foam core thicknesses of the severely damaged frontal components. The proposed designs can efficiently change the load path and enhance energy transfer from the impact point to the other structural components. Thus, the intrusion of the structure into the residual space and the occupant injury risks were substantially mitigated with a minimal weight increment. Finally, based on the characteristics of adjusting the thicknesses of the four frontal components, a simple method for developing an alternative design of a lightweight bus structure integrated with safety purposes was provided.

Declarations

Author contribution statement

Pattaramon Jongpradist, Sontipee Aimmanee: Conceived and designed the experiments; Analyzed and interpreted the data; Contributed reagents, materials, analysis tools or data; Wrote the paper. Napassakorn Saingam: Conceived and designed the experiments; Performed the experiments; Analyzed and interpreted the data; Wrote the paper. Ploypimol Tangthamsathit, Panittha Chanpaibool: Conceived and designed the experiments; Performed the experiments; Analyzed and interpreted the data. Jariyavadee Sirichantra: Conceived and designed the experiments; Performed the experiments; Contributed reagents, materials, analysis tools or data.

Funding statement

Pattaramon Jongpradist was supported by Thailand Science Research and Innovation [Basic Research Fund: Fiscal year 2022 FRB650048/0164].

Data availability statement

Data will be made available on request.

Declaration of interests statement

The authors declare no conflict of interest.

Additional information

No additional information is available for this paper.

Appendix A

The composite material model used in LS-DYNA was verified following the ASTM D7136 Standard Test Method for Measuring the Damage

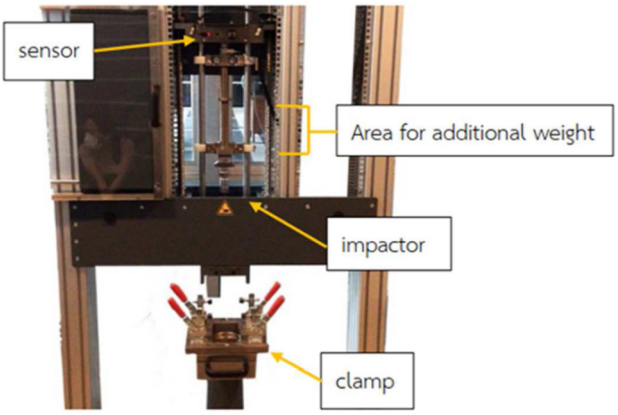

Fig. A.1. Zwick Roell HIT230F drop-weight impact testing machine.

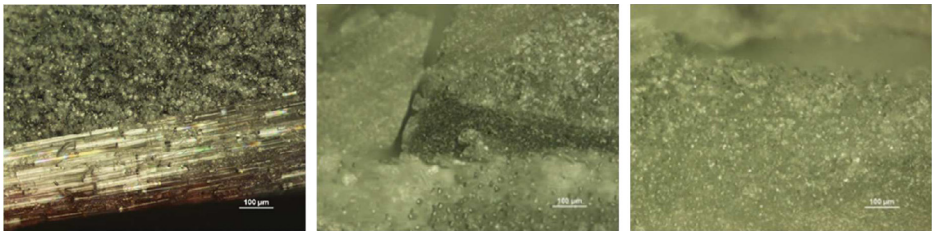

Fig. A.2. Microstructural observation of failure modes of composite plates under the drop-weight impact test; (a) fiber breakage, (b) matrix cracking, (c) delamination.

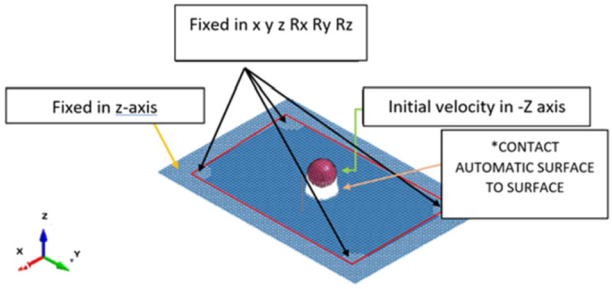

Fig. A.3. Finite element setup of the impact test on the composite plate.

*MAT_ENHANCED_COMPOSITE_DAMAGE_(TITLE) (054/055) (3)

	TITLE							
	G400							
1	MID	RO	EA	EB	(EC)	PRBA	(PRCA)	(PRCB)
	2	1.588e-006	18.040001	18.040001	0.0	0.1000000	0.0	0.0
2	GAB	GBC	GCA	(KF)	AOPT	2WAY		
	2.2190001	2.2190001	0.0	0.0	0.0	1.0000000		
3	XP	YP	ZP	A1	A2	A3	MANGLE	
	0.0	0.0	0.0	0.0	0.0	0.0	0.0	
4	V1	V2	V3	D1	D2	D3	DFAILM	DFAILS
	0.0	0.0	0.0	0.0	0.0	0.0	1.0000000	1.0000000
5	TFAIL	ALPH	SOFT	FBRT	YCFAC	DFAILT	DFAILC	EFS
	0.0	0.0	1.0000000	1.0000000	1.0000000	1.0000000	-1.0000000	0.0
6	XC	XT	YC	YT	SC	CRIT	BETA	
	0.2000000	0.4150000	0.2000000	0.4150000	0.0750000	54.0	0.5000000	
7	PEL	EPSF	EPSR	TSMD	SOFT2			
	0.0	0.0	0.0	0.0	1.0000000			
8	SLIMT1	SLIMC1	SLIMT2	SLIMC2	SLIMS	NCYRED	SOFTG	
	1.0000000	1.0000000	1.0000000	1.0000000	1.0000000	0.0	1.0000000	
9	LCXC	LCXT	LCYC	LCYT	LCSC	DT		
	0	0	0	0	0	0.0		

Fig. A.4. Properties of fiberglass G400 in MAT054 card.

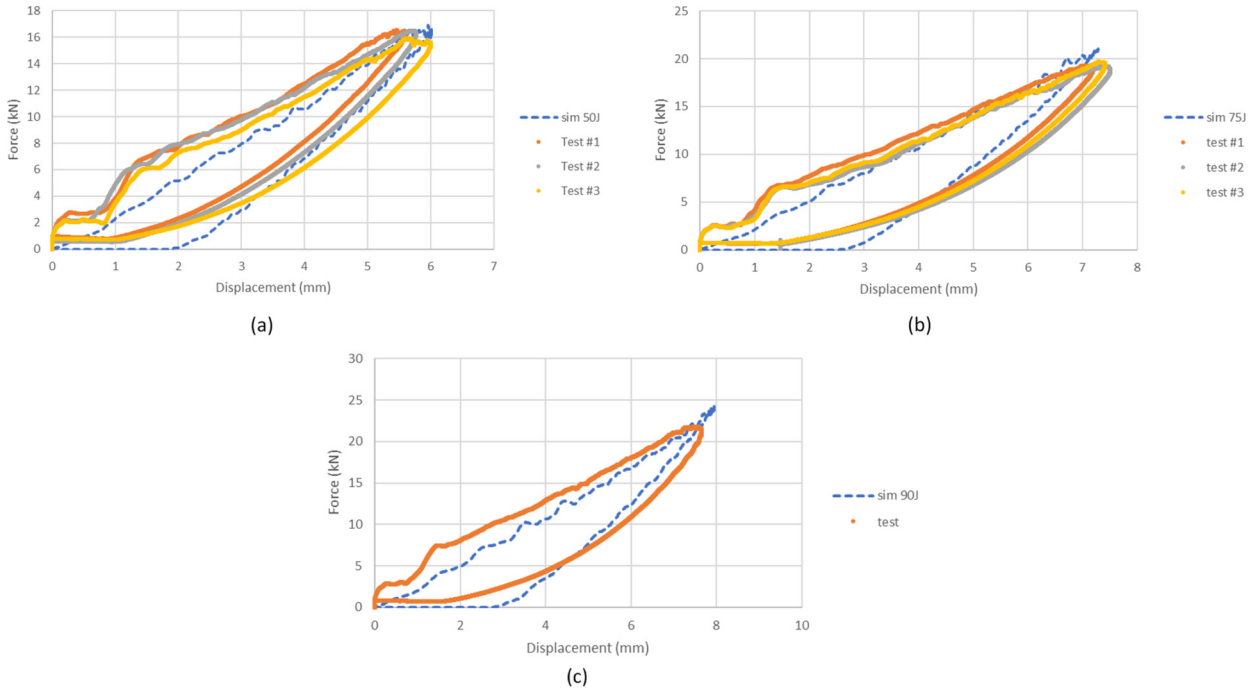

Fig. A.5. Comparisons of the force-displacement curve between the experimental and simulation results; (a) 50 J, (b) 75 J, (c) 90 J.

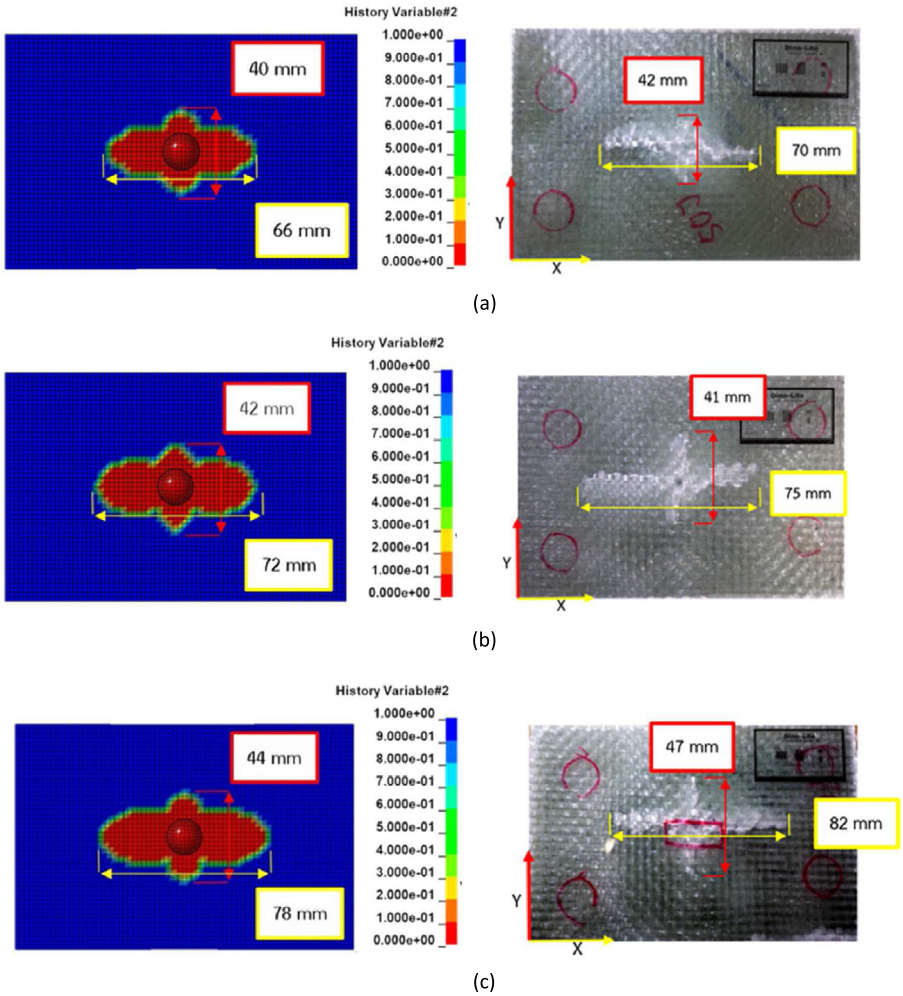

Fig. A.6. Comparisons of damage in the compressive fiber mode between the experimental and simulation results; (a) 50 J, (b) 75 J, (c) 90 J.

Resistance of a Fiber-Reinforced Polymer Matrix Composite to a Drop-Weight Impact Event. The impact testing machine used to collect data was a Zwick Roell HIT230F with a 16-millimeter hemispherical steel impactor tip, as shown in Fig. A.1. Composite plate specimens were 100 x 150 square millimeters in planform dimension and composed of 6 plies of 0/90 woven fiberglass G400 and 8 plies of ±45 woven fiberglass G400. The specimens were fabricated by a vacuum infusion process and tested under 50 J, 70 J, and 90 J.

The damage distribution of the specimens was examined intimately using a Nikon ECLIPSE LV 150N optical microscope (Nikon; Melville, NY, USA). Fig. A.2 shows that there are three main damage modes observed, including fiber breakage, matrix cracking, and delamination.

The finite element model was developed to simulate the damage and deformation of the composite plate in LS-DYNA. Fig. A.3 shows the setup of the impact test on the composite plate. The 100×150 mm^2 plate was discretized by rectangular-shaped shell elements. The composite layer and fiber orientation were defined in *PART COMPOSITE. Mechanical properties of woven glass fiber were assigned in *MAT ENHANCE COMPOSITE DAMAGE (MAT054). However, there were some parameters we could not specify from the experiment that could have a significant effect. Ning et al. examined the impact of the SLIM parameter presented in MAT LAMINATED COMPOSITE FABRIC (MAT058), which resembles MAT054, to investigate the numerical impact on a Formula Student racing car carbon composite nose cone. They compared numerical models to experimental data discussed in deceleration accuracy and concluded that SLIM is an essential factor in determining the minimum stress limit after failure. According to their suggestion, all SLIM parameters in the present study were set to 1.0 to meet the required accuracy. The mechanical properties and other parameters of glass fiber G400 in MAT054 are shown in Fig. A.4.

The force-displacement curves of the composite plate obtained from the finite element method and the impact experiment are plotted in Fig. A.5. The area under the graph represents residual internal energy due to material damage. In other words, energy absorption. A comparison of the results from the experiment and finite element analysis indicates that the energy absorption obtained from both methods is in good agreement with the differences of less than 10%.

Apart from the force-displacement curves, material damage failure modes were also observed. Fiber breakages were noticed on compression and tension faces using an optical microscope. The largest one seen with the naked eye was the crack path on the top of the plate. The crack path length along both the x- and y-axes was then measured and compared with the simulation result from History variable #2, which presents the compressive fiber mode. As shown in Fig. A.6, the results from the experiment agreed well with the finite-element method.

References

Standard Test Method for Measuring the Damage Resistance of a Fiber-Reinforced Polymer Matrix Composite to a Drop-Weight Impact Event.

Chu, S., Majumdar, A., 2012. Opportunities and challenges for a sustainable energy future. Nature 488 (7411), 294–303.

Fantuzzi, N., et al., 2021. The use of sustainable composites for the manufacturing of electric cars. Composites, Part C: Open Access 4, 100096.

Hartley, J.W., 2018. Crashworthiness Improvements to Automotive Sandwich Composites Using Tufting. (Ph.D. thesis).

Jongpradist, P., et al., 2021. Crash analysis of sandwich composite electric microbus. IOP Conf. Ser., Mater. Sci. Eng. 1137 (1), 012048.

Jongpradist, P., Senawat, S., Muangto, B., 2015. Improvement of crashworthiness of bus structure under frontal impact. Adv. Struct. Eng. Mech. ASEM15, 1–11.

Joost, W.J., 2012. Reducing vehicle weight and improving US energy efficiency using integrated computational materials engineering. J. Minerals, Metals & Materials Soc. (TMS) 64, 1032–1038.

Kongwat, S., Jongpradist, P., Hasegawa, H., 2020. Lightweight bus body design and optimization for rollover crashworthiness. Int. J. Automot. Technol. 21 (4), 981–991.

Kunakorn-ong, P., et al., 2020. Design and optimization of electric bus monocoque structure consisting of composite materials. Proc. Inst. Mech. Eng., Part C, J. Mech. Eng. Sci. 234 (20), 4069–4086.

Kunakorn-ong, P., Jongpradist, P., 2020. Optimisation of bus superstructure for rollover safety according to ECE-R66. Int. J. Automot. Technol. 21 (1), 215–225.

Kwasniewski, L., et al., 2009. Crash and safety assessment program for paratransit buses. Int. J. Impact Eng. 36 (2), 235–242.

LS-DYNA, 2020. Keyword User's Manual R13.0, Livermore. Software Technology Corporation, Livermore, USA.

Luk, J.M., et al., 2017. Review of the fuel saving, life cycle GHG emission, and ownership cost impacts of lightweighting vehicles with different powertrains. Environ. Sci. Technol. 51 (15), 8215–8228.

de Meira, A.D., et al., 2016. Numerical analysis of an intercity bus structure: a simple unifilar model proposal to assess frontal and semifrontal crash scenarios. Lat. Am. J. Solids Struct. 13 (9), 1616–1640.

National Highway Traffic Safety Administration (2021), 2019 Traffic Safety Facts a Compilation of Motor Vehicle Crash Data (Annual FARS/GES/CRSS Report), p. 242.

National Highway Traffic Safety Administration (2011), Federal Motor Vehicle Safety Standard (FMVSS). No. 208- Occupant Crash Protection.

Ning, H., et al., 2007. Thermoplastic sandwich structure design and manufacturing for the body panel of mass transit vehicle. Compos. Struct. 80 (1), 82–91.

Pavlović, A., et al., 2020. On the modal behaviour of ultralight composite sandwich automotive panels. Compos. Struct. 248.

Regulation No. 29 of the economic commission for Europe of the United Nations. In: Occupant Protection in Cabs of Commercial Vehicles.

Regulation No. 66 of the Economic Commission for Europe of the United Nations. In: Large Passenger Vehicles with Regard to the Strength of Their Superstructure.

Seyedi, M.R., et al., 2019. Experimental assessment of vehicle performance and injury risk for cutaway buses using tilt table and modified dolly rollover tests. Accid. Anal. Prev. 132, 105287.

Tarlochan, F., Ramesh, S., Harpreet, S., 2012. Advanced composite sandwich structure design for energy absorption applications: blast protection and crashworthiness. Composites, Part B, Eng. 43 (5), 2198–2208.

Testoni, O., 2015. Concept and Preliminary Design of a Composite Monocoque for an Electric City-Bus. MS thesis. ETH-Zürich.

Wang, Z.W., Zhao, J.P., Zhang, X., 2018. Finite element analysis of composite laminates subjected to low-velocity impact based on multiple failure criteria. Mater. Res. Express 5 (6).